DOI: https://doi.org/10.62985/j.huit_ojs.vol26.no2E.424

EXPERIMENTAL EVALUATION OF CLASSICAL BACKSTEPPING AND RBF NEURAL NETWORK BASED BACKSTEPPING ON AN INVERTED PENDULUM SYSTEM

Khuong Huynh Van[1,*], Anh Nguyen The[1], Xuan Bui Thanh[1], Thang Doan Cong[2]

[1]*Naval Academy, Nha Trang, Vietnam*

[2]*Air Force Officer's College, Nha Trang, Vietnam*

*Email: *hvkhuongautomation@gmail.com*

Received: 20 December 2025; Revised: 21 March 2026; Accepted: 16 April 2026

ABSTRACT

This paper presents an experimental comparison between the classical Backstepping controller and an improved Backstepping design incorporating Radial Basis Function (RBF) neural networks on an inverted pendulum system. While the conventional Backstepping method ensures stability based on a known mathematical model, its performance is sensitive to parameter uncertainties and unmodeled nonlinearities. The RBF-enhanced Backstepping controller addresses these limitations by compensating for unknown dynamics through real-time neural network approximation. Experimental results on an STM32F4 embedded platform indicate that the Backstepping-RBF controller achieves faster stabilization, reduced oscillations, and smoother control signals compared with the classical Backstepping method.

Keywords: Backstepping, RBF neural networks, nonlinear control, inverted pendulum.

1. INTRODUCTION

The inverted pendulum is one of the most classical and challenging benchmark systems in nonlinear control due to its strong nonlinear characteristics and high sensitivity to model parameter variations. This system has been widely used in research as it reflects many important features of practical control engineering systems, such as overhead cranes transporting heavy loads, missile attitude deviation during launch, and bipedal walking robots, where linear models are inherently inadequate. The control objective is to maintain the pendulum in its unstable upright equilibrium position while ensuring that the cart motion remains within allowable limits.

Over the past decades, the inverted pendulum control problem has been addressed using various approaches. Traditional linear controllers such as PID and LQR offer simplicity and ease of implementation; however, their performance degrades significantly when the system operates far from the equilibrium point or in the presence of model uncertainties and external disturbances. In practical inverted pendulum systems, factors such as friction, motor dynamics, measurement errors, and hardware constraints make accurate modeling difficult, thereby reducing the effectiveness of linear control methods.

To overcome these limitations, numerous nonlinear control strategies have been developed, including feedback linearization, sliding mode control, and the Backstepping approach. Among them, the Backstepping method is highly regarded for its systematic design procedure and its ability to guarantee stability based on Lyapunov theory. Nevertheless, classical Backstepping depends on the accuracy of the mathematical model and is therefore sensitive to parameter variations and unmodeled dynamics.

In recent years, intelligent and adaptive control techniques - particularly those incorporating RBF neural networks - have demonstrated great potential in handling nonlinear systems with uncertainties. Owing to their capability to approximate unknown nonlinear functions, RBF neural networks can be integrated into the Backstepping framework to compensate for modeling errors in real time and enhance system robustness. The effectiveness of the Backstepping controller combined with RBF neural networks has been demonstrated through theoretical analysis [9] and experimental investigations on inverted pendulum systems [11].

However, most existing studies focus on proposing and validating the performance of Backstepping-RBF controllers, while direct experimental comparisons between classical Backstepping and Backstepping-RBF implemented on the same hardware platform remain limited. The lack of such comparative studies makes it difficult to quantitatively assess the practical benefits of incorporating neural networks into the Backstepping structure.

Motivated by this observation, this paper does not aim to propose a new control method, but rather focuses on supplementing and presenting detailed experimental results of the classical Backstepping controller implemented on the same inverted pendulum system and the same STM32F4 embedded platform. Based on these results, a direct experimental comparison is conducted between the classical Backstepping controller and the previously published Backstepping-RBF controller [11]. The comparison criteria include stabilization time, system oscillations, and control signal characteristics, thereby clarifying the practical advantages of integrating RBF neural networks under real operating conditions.

2. INVERTED PENDULUM SYSTEM MODEL

The inverted pendulum system considered in this paper (Fig. 1) consists of a pendulum rod (which can be equipped with an additional mass) mounted on a cart moving horizontally, where the pendulum is free to rotate about a joint connected to the cart. The system is driven by a DC motor through a ball-screw transmission mechanism that generates the driving force acting on the cart.

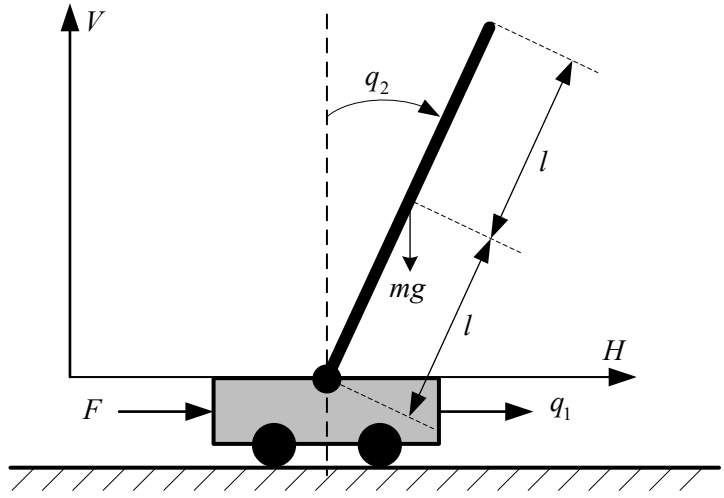

Fig. 1. Inverted pendulum system model

Let q_1 denote the position of the cart and q_2 denote the angle of the pendulum with respect to the vertical direction. When $q_2 = 0$, the pendulum is at the unstable upright

equilibrium position; when $q_2 = \pi$, the pendulum is in the downward position [11]. Based on these definitions, the state variables of the system are defined as:

$$x_1 = q_1, \quad x_2 = q_2, \quad x_3 = \dot{q}_1, \quad x_4 = \dot{q}_2$$

The state vector of the inverted pendulum system is given by:

$$\boldsymbol{x} = [x_1, x_2, x_3, x_4]^T$$

Using the Lagrange method, the nonlinear dynamics of the inverted pendulum system can be derived in the form of second-order differential equations. Detailed derivations of the system model and dynamic analysis have been presented in previous work [1]. Accordingly, the system dynamics can be expressed in state-space form as follows:

$$\begin{cases} \dot{x}_1 = x_3 \\ \dot{x}_2 = x_4 \\ \dot{x}_3 = \dfrac{\left(J + ml^2\right)\left(mlx_4^2 \sin x_2 - kx_3\right) - ml\cos x_2\left(mgl\sin x_2 - cx_4\right) + \left(J + ml^2\right)F}{\left(M + m\right)\left(J + ml^2\right) - m^2l^2\left(\cos x_2\right)^2} \\ \dot{x}_4 = \dfrac{\left(M + m\right)\left(mgl\sin x_2 - cx_4\right) - ml\cos x_2\left(mlx_4^2 \sin x_2 - kx_3\right) - ml\cos x_2 F}{\left(M + m\right)\left(J + ml^2\right) - m^2l^2\left(\cos x_2\right)^2} \end{cases} \quad (1)$$

where $M(kg)$ is the mass of the cart, $m(kg)$ is the mass of the pendulum rod, $l(m)$ is the distance from the rotation axis to the center of mass of the pendulum, $g(m/s^2)$ is the gravitational acceleration, $F(N)$ is the control force applied to the cart, k is the friction coefficient between the cart and the rail, c is the friction coefficient at the pendulum pivot, and $J(kg.m^2)$ is the moment of inertia of the pendulum about its center of mass.

Assume that the force applied to the cart is given as follows:

$$F = \frac{2\pi\eta K_m K_g}{pR}u_t - \frac{(2\pi)^2\eta K_m^2 K_g^2}{p^2 R}\dot{x} = K_u u_t - K_x x_3 \quad (2)$$

where u_t is the voltage applied to the DC motor to generate the driving force acting on the cart, $K_m(N.m/A)$ is the motor torque constant, K_g is the motor gearbox transmission ratio, $R(\Omega)$ is the armature resistance of the motor, $p(m/rev)$ is the lead of the ball screw (the linear displacement per revolution), η is the efficiency of the ball-screw mechanism.

By combining (1) and (2), we obtain:

$$\begin{cases} \dot{x}_1 = x_3 \\ \dot{x}_2 = x_4 \\ \dot{x}_3 = f_3(\boldsymbol{x}) + g_3(\boldsymbol{x})u_t \\ \dot{x}_4 = f_4(\boldsymbol{x}) + g_4(\boldsymbol{x})u_t \end{cases} \quad (3)$$

where,

$$f_3\left(\boldsymbol{x}\right) = \frac{\left(J + ml^2\right)\left(mlx_4^2 \sin x_2 - kx_3\right) - ml\cos x_2\left(mgl\sin x_2 - cx_4\right) - \left(J + ml^2\right)\left(K_x x_3\right)}{\left(M + m\right)\left(J + ml^2\right) - m^2l^2\left(\cos x_2\right)^2} \quad (4)$$

$$g_3(\boldsymbol{x}) = \frac{\left(J + ml^2\right)K_u}{\left(M+m\right)\left(J+ml^2\right) - m^2l^2\left(\cos x_2\right)^2} \tag{5}$$

$$f_4(\boldsymbol{x}) = \frac{\left(M+m\right)\left(mgl\sin x_2 - cx_4\right) - ml\cos x_2\left(mlx_4^2\sin x_2 - kx_3\right) + ml\cos x_2\left(K_x x_3\right)}{\left(M+m\right)\left(J+ml^2\right) - m^2l^2\left(\cos x_2\right)^2} \tag{6}$$

$$g_4(\boldsymbol{x}) = \frac{-ml\cos x_2 K_u}{\left(M+m\right)\left(J+ml^2\right) - m^2l^2\left(\cos x_2\right)^2} \tag{7}$$

In the theoretical model, the system parameters include the cart mass, the pendulum mass, the pendulum length, the moment of inertia, friction coefficients, and motor constants. However, under practical operating conditions, these parameters are often difficult to identify accurately, and in particular, some parameters may vary over time during operation. These factors lead to discrepancies between the mathematical model and the actual system, directly affecting the performance of model-based controllers.

In this paper, the mathematical model of the inverted pendulum system is used as the basis for designing the classical Backstepping controller. Subsequently, the present study focuses on supplementing the experimental results of the classical Backstepping controller and conducting a direct experimental comparison with the Backstepping controller combined with an RBF neural network that has been previously published [11].

3. SYNTHESIS OF THE BACKSTEPPING CONTROL LAW

This section presents a brief summary of the classical Backstepping controller and the Backstepping controller combined with an RBF neural network used in the experimental comparison. The purpose of this section is to provide a clear basis for the implementation and experimental evaluation of the controllers, rather than to propose a new control method. Detailed design procedures of the controllers have been presented in the authors' previous work [11].

The block diagrams of the inverted pendulum control system using the classical Backstepping controller and the Backstepping controller combined with an RBF neural network are illustrated in Fig. 2 and Fig. 3, respectively. Based on Equations (16) and (17) reported in [11], the classical Backstepping control law and the Backstepping-RBF control law are determined as follows.

$$u_t = \frac{1}{g_4 - k_1 g_3}\left[k_1 f_3 - f_4 - c_1\left(x_4 - k_1 x_3\right) - e_1 - c_2 e_2\right] \tag{8}$$

Equation (8) represents the classical Backstepping control law, in which the nonlinear functions f_3, g_3, f_4, and g_4 are determined from (4), (5), (6), and (7), respectively.

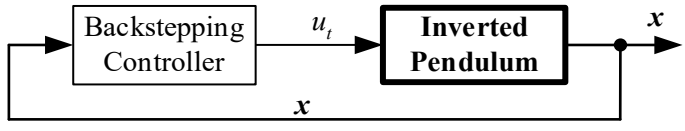

Fig. 2. Classical Backstepping control of the inverted pendulum system

$$u_t = \frac{1}{\left(\hat{g}_4 - k_1\hat{g}_3\right)}\left[k_1\hat{f}_3 - \hat{f}_4 - c_1\left(x_4 - k_1 x_3\right) - e_1 - c_2 e_2\right] \tag{9}$$

Equation (9) represents the Backstepping-RBF control law, where $\hat{f}_3$, $\hat{g}_3$, $\hat{f}_4$, and $\hat{g}_4$ denote the estimated values of f_3, g_3, f_4, and g_4, respectively, provided by the RBF neural network through an adaptive mechanism. Detailed descriptions of the network structure, adaptive law, and stability analysis have been fully presented in [11].

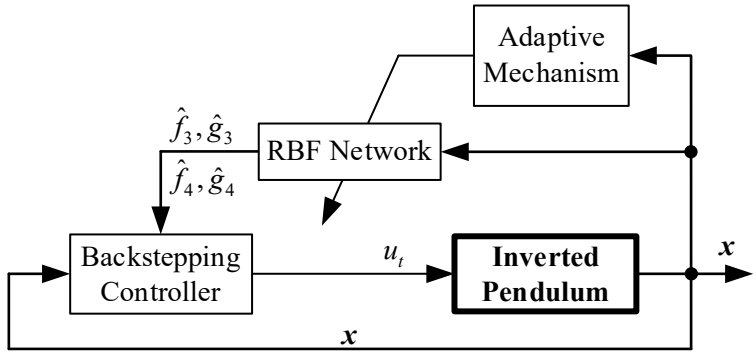

Fig. 3. Backstepping-RBF control of the inverted pendulum system

4. EXPERIMENTAL RESULTS

This experimental section focuses on evaluating and comparing two control laws, namely the classical Backstepping (8) and the Backstepping-RBF (9), based on their responses in driving the pendulum angle q_2 toward zero within the limited travel range of the cart. The initial pendulum angle for applying control laws (8) and (9) is selected as $|q_2| = \pi/12(rad)$. It should be noted that, during the experimental implementation of control law (8), the pendulum mass of 84 (g) is kept constant across all experimental cases. In addition, some system model parameters are estimated by the authors rather than being accurately identified, such as the motor-related parameters.

4.1. Experimental Model and Data Acquisition Software

Fig. 4 shows the experimental setup of the inverted pendulum system. The system consists of a pendulum rod with adjustable mass, a cart with a mass of 712 (g), a DC motor, and an STM32F407 microcontroller that executes the control algorithms and transmits the collected data to a computer for visualization. Encoders are used to measure the pendulum angle and the cart position.

The data acquisition software interface is illustrated in Fig. 5, which displays the time responses of the system states, including the pendulum angle, the cart position, and the control signal u_t. Detailed descriptions of the experimental setup and the data acquisition software have been fully presented in [11].

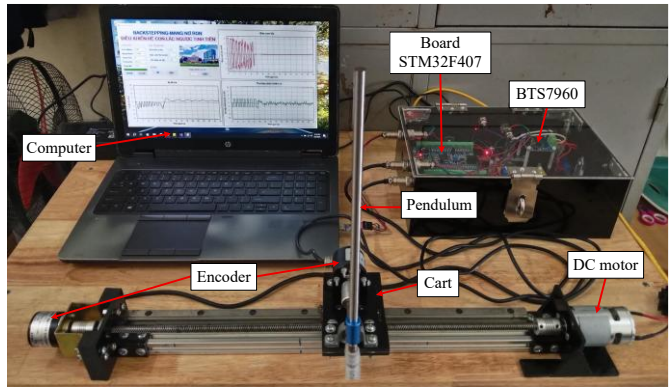

Fig. 4. Experimental model of the inverted pendulum system

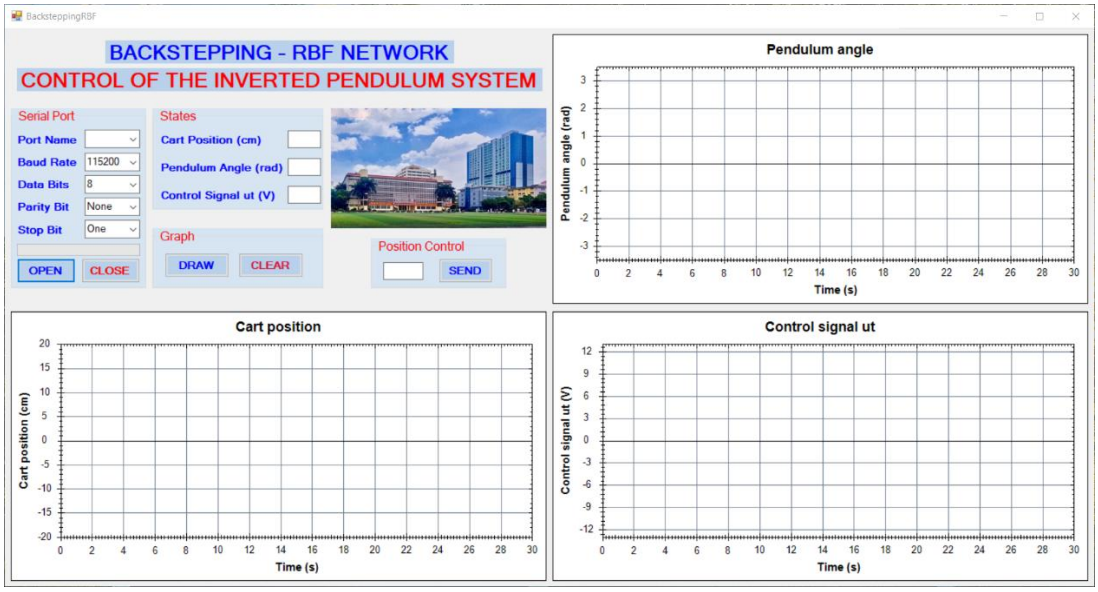

Fig. 5. Data acquisition software interface

4.2. Experimental Data

To evaluate and compare the performance of control laws (8) and (9), the experiments were conducted on the same inverted pendulum system and using the same hardware platform. The experiments were carried out under multiple test scenarios while maintaining identical operating conditions in order to ensure the objectivity and fairness of the comparison process.

4.2.1. Case 01, cylindrical pendulum rod with a mass of 84 (g)

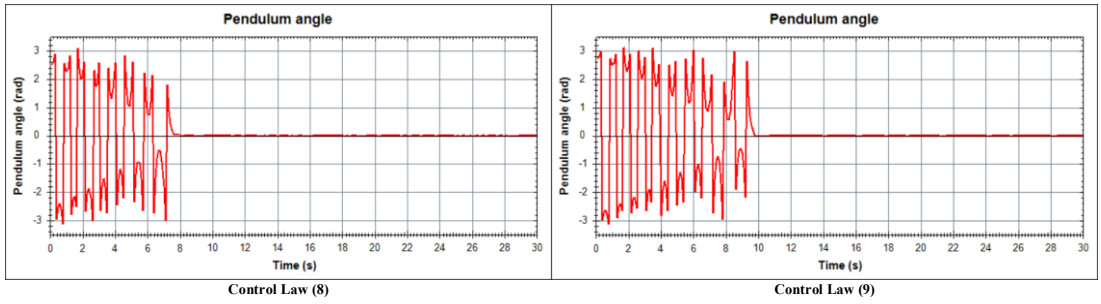

Fig. 6. Pendulum angle response under control laws (8) and (9)

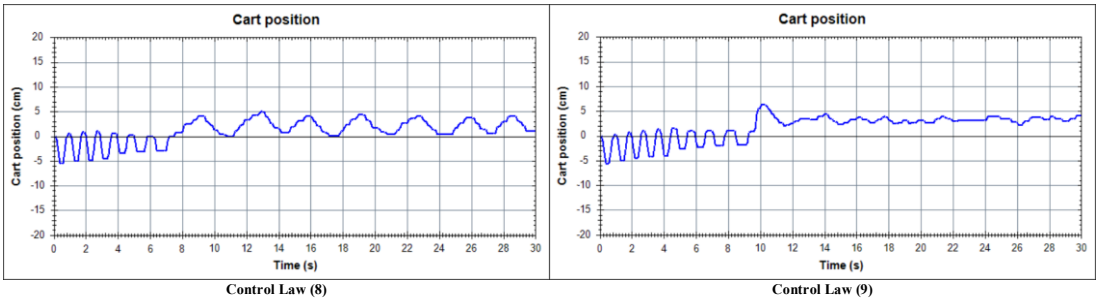

Fig. 7. Cart position response under control laws (8) and (9)

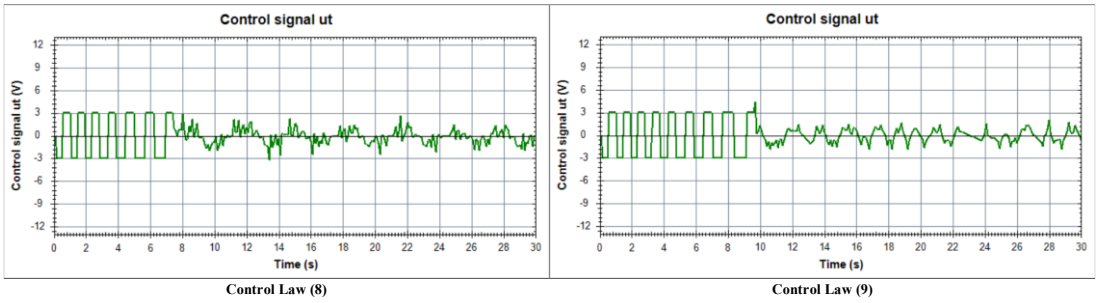

Fig. 8. Control input under control laws (8) and (9)

4.2.2. Case 02, cylindrical pendulum rod with a mass of 126 (g)

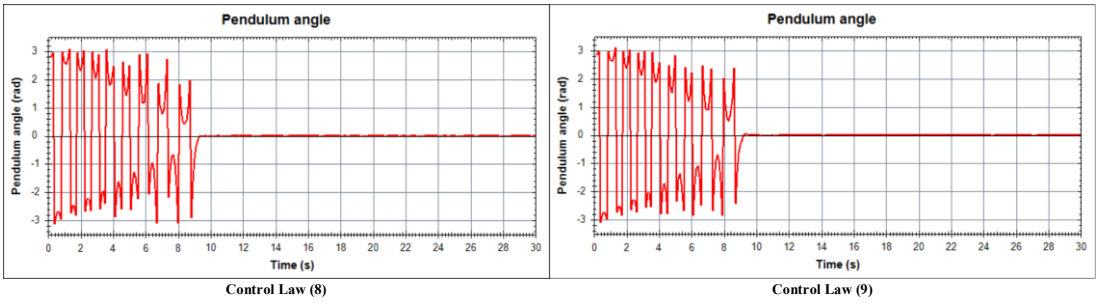

Fig. 9. Pendulum angle response under control laws (8) and (9)

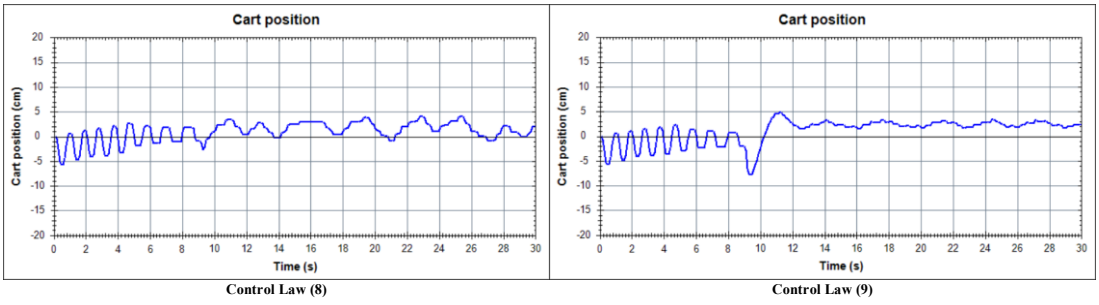

Fig. 10. Cart position response under control laws (8) and (9)

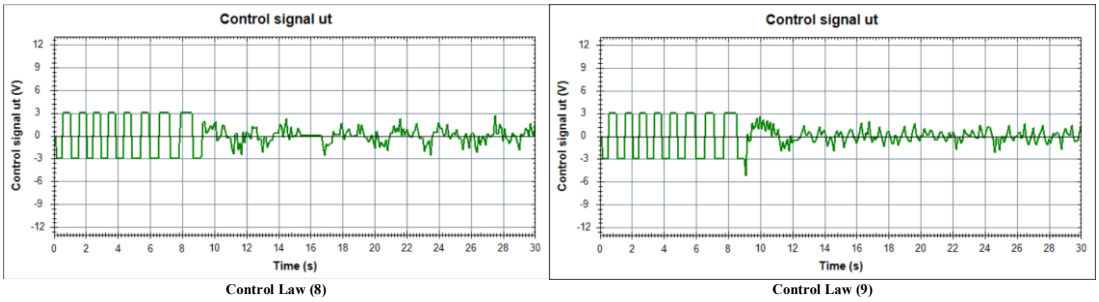

Fig. 11. Control input under control laws (8) and (9)

4.2.3. Case 03, cylindrical pendulum rod with an additional payload, total mass of 502 (g)

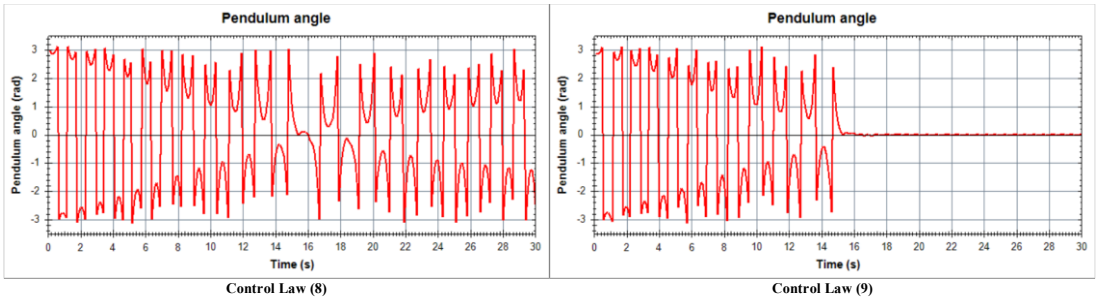

Fig. 12. Pendulum angle response under control laws (8) and (9)

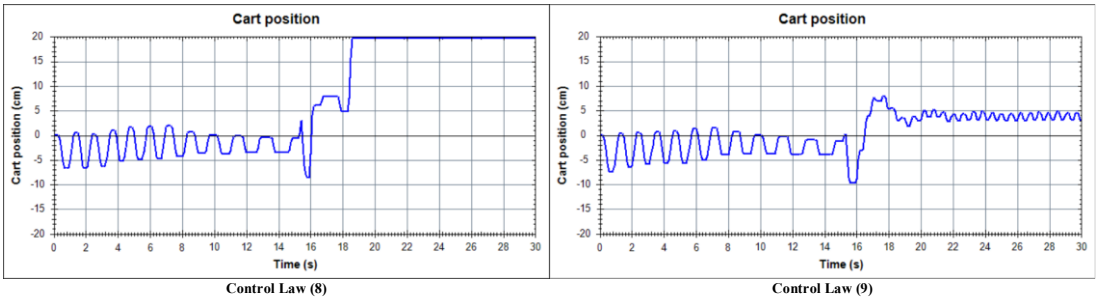

Fig. 13. Cart position response under control laws (8) and (9)

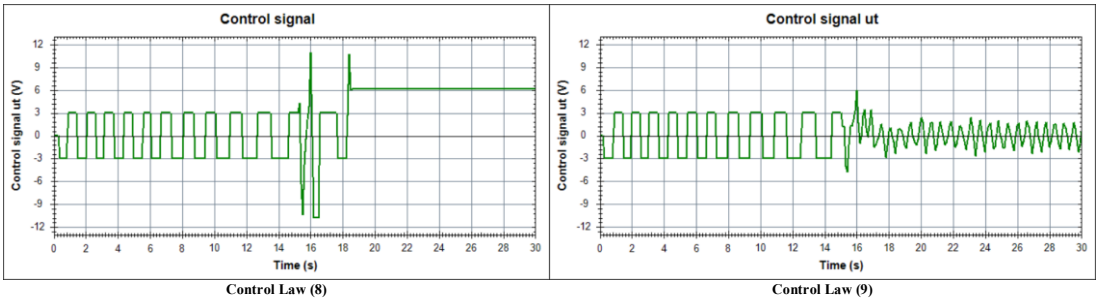

Fig. 14. Control input under control laws (8) and (9)

4.3. Discussion of Experimental Results

The following discussion focuses only on the experimental data obtained from control laws (8) and (9), and does not include the data related to the swing-up controller.

Table 1. Evaluation of pendulum angle response

Experimental cases	Quality criteria for the pendulum angle response			
	Time for pendulum angle to converge from $\lvert q_2 \rvert = \pi / 12(rad)$ *to 0*		*Stability of the angle after* q_2 *converges to 0*	
	Law (8)	*Law (9)*	*Law (8)*	*Law (9)*
Case 1	0.4 (s)	0.2 (s)	High oscillation	Low oscillation
Case 2	0.2 (s)	0.2 (s)	High oscillation	Low oscillation
Case 3	Loss of control	0.2 (s)	Loss of control	High oscillation

Table 2. Evaluation of cart position response

Experimental cases	Quality criteria for the cart position response					
	Average value		*Oscillation amplitude*		*Maximum distance from the initial cart position*	
	Law (8)	*Law (9)*	*Law (8)*	*Law (9)*	*Law (8)*	*Law (9)*
Case 1	2.2 (cm)	3.2 (cm)	2.0 (cm)	0.9 (cm)	5.0 (cm)	6.5 (cm)
Case 2	1.6 (cm)	2.5 (cm)	2.6 (cm)	0.9 (cm)	4.2 (cm)	7.8 (cm)
Case 3	Loss of control	3.7 (cm)	Loss of control	0.9 (cm)	Reached travel limit	9.9 (cm)

Table 3. Evaluation of control signal

Experimental cases	Quality criteria for the control signal u_t			
	Maximum voltage amplitude		*Frequency*	
	Law (8)	*Law (9)*	*Law (8)*	*Law (9)*
Case 1	3.1 (V)	4.4 (V)	High	Low
Case 2	2.7 (V)	5.1 (V)	High	Low
Case 3	Loss of control	6.0 (V)	Loss of control	Low

For the pendulum angle response, the experimental results show that in the cases of small and medium pendulum masses (Case 1 and Case 2), both control laws are capable of driving the pendulum angle q_2 the equilibrium position $q_2 = 0$. However, the Backstepping–RBF controller (9) exhibits a faster convergence time (Case 1) or a comparable convergence time (Case 2) compared to the classical Backstepping controller (8), while achieving a significantly smaller level of oscillation after stabilization.

Notably, in Case 3, when the pendulum mass increases to a large value (502 g), the classical Backstepping controller (8) can no longer maintain system stability, leading to loss of control. In contrast, the Backstepping–RBF controller (9) is still able to stabilize the system with a convergence time of approximately 0.2 (s), demonstrating superior robustness against system parameter variations.

For the cart position response, the experimental results indicate that the Backstepping–RBF controller (9) significantly reduces the oscillation amplitude of the cart compared to the classical Backstepping controller (8) in all three tested cases. In Case 1 and Case 2, although the average cart position under control law (9) tends to be larger, the oscillation amplitude is considerably smaller than that obtained with control law (8). This observation indicates that the cart motion under control law (9) is more stable and exhibits reduced oscillations.

In Case 3, the classical Backstepping controller (8) is no longer able to regulate the cart motion, resulting in the cart reaching the travel limit. In contrast, the Backstepping–RBF controller (9) maintains the cart motion within the allowable range, although the maximum displacement of the cart from its initial position increases to 9.9 cm. This result reflects a reasonable trade-off between pendulum stabilization and cart motion when the system is subject to significant uncertainties.

Regarding the control signal u_t, the Backstepping–RBF controller (9) exhibits a larger peak voltage amplitude than the classical Backstepping controller (8) in the cases where control is successfully maintained. However, the control signal generated by control law (9) is smoother, more stable, and less oscillatory, which helps reduce adverse effects on the actuator. In contrast, the control signal of control law (8) exhibits high-frequency oscillations.

In Case 3, when control law (8) loses stability, control law (9) is still able to generate a stable control signal with low frequency, demonstrating the effective adaptive capability of the RBF neural network in compensating for model uncertainties.

5. CONCLUSION

When the dynamic characteristics of the inverted pendulum system are accurately known, both the classical Backstepping controller (8) and the Backstepping controller combined with an RBF neural network (9) are able to guarantee the stability of the system at the unstable equilibrium point, $q_2 = 0$.

However, in the presence of large variations in the pendulum mass (specifically, when the pendulum mass increases by a factor of six from 84 (g) to 502 (g)) or when significant model uncertainties exist, the adaptive control law (9) becomes superior due to its capability to approximate unknown nonlinear functions using the RBF neural network. This enables the system to maintain stable operation without requiring precise knowledge of the system dynamics, which cannot be achieved by the classical Backstepping controller.

Future research directions include combining the RBF neural network with sliding mode control to enhance disturbance rejection capability and reduce response time, as well as investigating the influence of system delays – particularly delays associated with the DC motor and drive transmission. In addition, incorporating adaptive laws for the RBF network parameters and exploring other neural network structures in control and automation applications are promising topics for further study.

REFERENCES

[1] F.-K. Tsai and J.-S. Lin, “Nonlinear control design of 360-degree inverted pendulum systems,” in *Proc. 4th Int. Conf. Control Autom. (ICCA)*, Montreal, Canada, 2003, pp. 634–638, doi: https://doi.org/10.1109/ICCA.2003.1595099.

[2] L. B. Prasad, B. Tyagi, and H. O. Gupta, “Optimal control of nonlinear inverted pendulum system using PID controller and LQR: Performance analysis without and with disturbance input,” *Int. J. Autom. Comput.*, vol. 11, no. 6, pp. 661–670, 2014, doi: https://doi.org/10.1007/s11633-014-0818-1

[3] T.-B. Dang *et al.,* “PID control for cart and pole system: Simulation and experiment,” *J. Fuzzy Syst. Control*, vol. 2, no. 1, pp. 29–35, 2024, doi: https://doi.org/10.59247/jfsc.v2i1.165

[4] D.-P. Hoang, “A survey of experimental LQR for cart and pole,” *J. Fuzzy Syst. Control*, vol. 2, no. 2, pp. 97–103, 2024, doi: https://doi.org/10.59247/jfsc.v2i2.211

[5] N. X. Chiem and H. N. Phan, "Design controller of the quasi-time optimization approach for stabilizing and trajectory tracking of inverted pendulum," *MATEC Web Conf.*, vol. 226, p. 02007, 2018, doi: https://doi.org/10.1051/matecconf/201822602007

[6] S. Irfan, A. Mehmood, M. T. Razzaq, and J. Iqbal, "Advanced sliding mode control techniques for inverted pendulum: Modelling and simulation," *Eng. Sci. Technol. Int. J.*, vol. 21, no. 4, pp. 753–759, 2018, doi: https://doi.org/10.1016/j.jestch.2018.06.010

[7] M. Mahmoud, R. Saleh, and A. Ma'arif, "Stabilizing of inverted pendulum system using robust sliding mode control," *Int. J. Robot. Control Syst.*, vol. 2, no. 2, pp. 230–239, 2022, doi: https://doi.org/10.31763/ijrcs.v2i2.594

[8] H.-G.-B. Pham, "Trajectories tracking control for rotary inverted pendulum using backstepping method," *J. Fuzzy Syst. Control*, vol. 3, no. 1, pp. 57–63, 2025, doi: https://doi.org/10.59247/jfsc.v3i1.276

[9] J. Liu, *Radial Basis Function (RBF) Neural Network Control for Mechanical Systems*. Berlin, Germany: Springer, 2013, doi: https://doi.org/10.1007/978-3-642-34816-7

[10] H. N. Phan and C. X. Nguyen, "Building embedded quasi-time-optimal controller for two-wheeled self-balancing robot," *MATEC Web Conf.*, vol. 132, p. 02005, 2017, doi: https://doi.org/10.1051/matecconf/201713202005

[11] H. V. Khuong, N. X. Chiem, and A. Obukhov, "Nonlinear control law design for inverted pendulum systems via RBF neural networks," *J. Fuzzy Syst. Control*, vol. 3, no. 2, pp. 164–169, 2025, doi: https://doi.org/10.59247/jfsc.v3i2.314

[12] U. Yildiran, "Adaptive control of an inverted pendulum by a reinforcement learning-based LQR method," *Sakarya Univ. J. Sci.*, 2023, doi: https://doi.org/10.16984/saufenbilder.1286391

[13] S. Irfan, L. Zhao, S. Ullah, A. Mehmood, and M. F. Butt, "Control strategies for inverted pendulum: A comparative analysis of linear, nonlinear, and artificial intelligence approaches," *PLOS ONE*, vol. 19, no. 3, Art. no. e0298093, 2024, doi: https://doi.org/10.1371/journal.pone.0298093